

Efficient Face Detection with Audio-Based Region Proposals

William Aris and François Grondin¹

Abstract—Robot vision often involves a large computational load due to large images to process in a short amount of time. Existing solutions often involve reducing image quality which can negatively impact processing. Another approach is to generate regions of interest with expensive vision algorithms. In this paper, we evaluate how audio can be used to generate regions of interest in optical images. To achieve this, we propose a unique attention mechanism to localize speech sources and evaluate its impact on a face detection algorithm. Our results show that the attention mechanism reduces the computational load. The proposed pipeline is flexible and can be easily adapted for human-robot interactions, robot surveillance, video-conferences or smart glasses.

I. INTRODUCTION

Computer vision in robotics is central to many applications ranging from autonomous navigation to human-robot interactions. However, due to the large amount of data to process in a short amount of time, i.e. thousands of pixels per frame, it often involves a large computational load. For example, many methods such as convolutional neural networks (CNN) [1], edge detection techniques [2] and the Viola-Jones face detector [3] rely on the convolution operation. Each convolution involves sliding a kernel along the image leading to a time complexity of approximately $\mathcal{O}(K^2HW)$ where K is the kernel size, H is the image height and W is the image width. While this is for one single convolution, most algorithms make use of multiple kernels, which further increases the number of computations. This can become a problem when working with high resolution images and/or low-cost embedded systems.

One way to tackle this challenge is to decrease the image resolution by using techniques such as nearest neighbor or bilinear interpolations. However, this often leads to a degradation of the image quality and introduces artifacts such as the "blocking" effect, which can negatively impact the performance of certain algorithms [4]. Another strategy consists in defining region proposals in the image and processing these regions with more expensive techniques. Selective search [5] and region proposal networks (RPN) [6], [7] are probably the most popular methods used for this purpose. Selective search first segments the image based on pixel intensity before grouping similar segments iteratively. Although this method has a high recall, it usually requires

several seconds to perform computations for a low-resolution image [8], [7], which makes real-time processing impossible. RPNs are often implemented as small sub-CNNs that take as input an image and output regions of interest (ROI) where the targeted objects could be. They tend to be faster than selective search and can run on low-cost hardware. However, this strategy still involves processing the entire image with convolution operations, which is not scalable. It's also worth mentioning that a third method, edge boxes [9], is faster than selective search but, according to the results reported in [8], fails to run in real-time.

Moreover, traditional region proposal techniques can determine *where* in an image a robot should engage its resources, but they ignore *when* it is worth doing so. It is often unnecessary for robots to continuously monitor a visual scene. For example, face detection becomes irrelevant when nobody faces the robot. Context awareness is key to share computing power amongst multiple processes and extend robot battery life.

This work demonstrates how sound can be used effectively to make region proposals in certain situations. Audio signals have the advantage of being represented by fewer data points than optical images while providing information redundancy at the semantic and spatial levels. For example, when a student asks a question in a classroom, the teacher can identify who is talking either with visual information, sound cues or both. The proposed pipeline aims to reduce the computational load in the context of human-robot interactions. Efficient and targeted face detection is crucial for natural human-robot interactions, therefore it represents a good use-case to orient this work. In addition, the pipeline can easily be adapted to other applications such as robot surveillance, video-conferences or smart glasses for the visually impaired.

The literature already reports techniques that use audio jointly with visual data. Both modalities are usually processed in parallel and late fusion increases detection robustness [10], [11], [12]. However, late fusion usually increases the computational load. To avoid redundancy, the alternative is to use the two modalities in cascade to complement one another. For example, an omnidirectional camera can be used to localize faces, whose positions are fed to a beamformer to find active speakers [13]. In [14], the authors go the other way around and use the direction of arrival of sound to select a static camera and perform face detection. Finally, in [15] an audio tracker is used to limit the search of a face detection algorithm. This work introduces two novel components: 1) we propose a method to determine when the robot should engage more resources in generating ROIs and 2) we introduce a time-frequency attention mechanism

*This work was supported in part by the Natural Sciences and Engineering Research Council of Canada - Collaborative Research and Training Experience program.

¹William Aris and François Grondin are with the Department of Electrical Engineering and Computer Engineering, Interdisciplinary Institute for Technological Innovation (3IT), 3000 boul. de l'Université, Université de Sherbrooke, Québec (Canada) J1K 0A5 {William.Aris, Francois.Grondin2}@USherbrooke.ca,

to localize the target speech source, and ignore undesirable interference.

This paper is organized as follows: Section II gives an overview of the system and explains the different design choices, Section III dives deeper in the implementation details of each module, Section IV presents the experimental results obtained and Section V concludes the paper and proposes avenues for future work.

II. PROPOSED PIPELINE

Figure 1 shows the global architecture of the system.

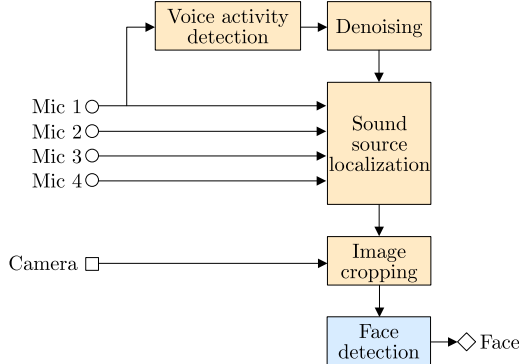


Fig. 1. Overview of the proposed pipeline. Each module can be tuned to fit to a specific application and the *face detection* block can be replaced by another task if necessary.

The pipeline first includes a simple voice activity detection (VAD) module to act as a gate-keeper. The module is here to add a layer of efficiency and indicate when the context is right to use the rest of the pipeline. If no voice is detected, it can be assumed that nobody wants to interact with the robot and the system can go in idle mode. Once voice is detected, audio is sent to the denoising module. Audio is often a mixture of the desired signal and noise which can degrade the localization performance. When the sound-to-noise (SNR) is low, it becomes essential to denoise the raw signal.

Finally, the localization module uses the denoised signal to localize voices and propose ROIs. Spatial information from audio can easily be derived using a microphone array and by exploiting the time difference of arrival (TDOA) of each microphone pair. The literature reports many sound source localization (SSL) techniques [16], [17], [18], each having pros and cons. The steered-beamformer based approach is particularly interesting in this case because the search space is well constrained by the image plane and the number of directions to look at can be parametrized to fit the requirements of specific situations (i.e., the resolution of the localization can be adjusted to save computation time without affecting the resolution of the optical image). By projecting the result of the steered-beamformer on an image plane, it is possible to generate acoustic images similar to figure 2.

Hence, the idea at the core of the pipeline is to select a region of interest around the peak of the acoustic image and only process this region with computer vision algorithms. An

interesting by-product of this mechanism is that it makes it possible to detect if a speaker is outside the field of view of the camera and to reorient the camera toward this person if necessary.

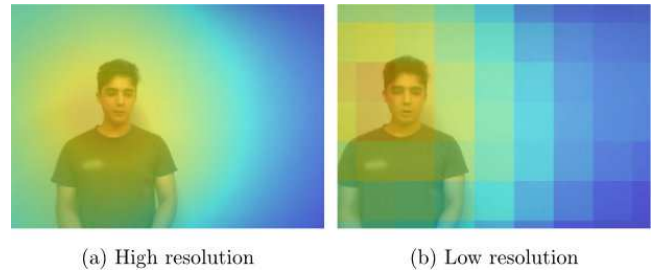


Fig. 2. Example of an acoustic images. An acoustic image can be seen as a heatmap showing where sound power lies with respect to an optical image. The resolution of the acoustic images can be adjusted without affecting the resolution of the optical images. Here (a) shows an acoustic image with a resolution of 640×480 regions while (b) has a resolution of 9×7 regions.

III. SYSTEM IMPLEMENTATION

A. Hardware

We design the low-cost acoustic camera shown in figure 3 for the project. The device is mainly based on an Arducam 1080p USB camera and a 4-channels ReSpeaker mic array. The housing is entirely 3D printed.

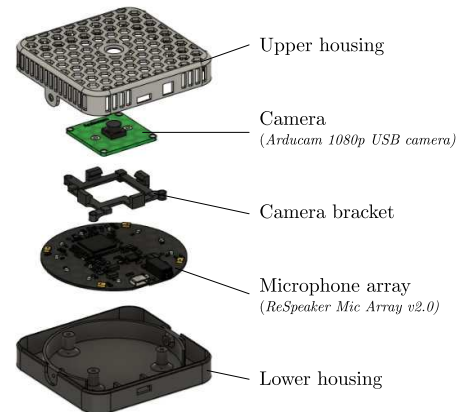


Fig. 3. Acoustic camera developed for the project.

To generate representative datasets when training neural networks, we measure 1000 multichannel room impulse responses (RIRs) with it. The RIRs are obtained using the exponential sine sweep (ESS) method proposed by Farina in [19] as it removes some distortions and offers a good SNR. When measuring the RIRs, a Bose SoundLink Flex loudspeaker generates 10 seconds ESSs going from 20 Hz to 8000 Hz. Recording is performed at a sample rate of 16 kHz and stops 3 seconds after the end of the signal to capture the late reverb. A total of 10 different rooms (100 samples per room) with different acoustic properties are sampled. The loudspeaker is moved between each measurement at random positions and the acoustic camera is moved between 3 to 4 times in each room.

This low-cost acoustic camera becomes a convenient tool for research in multimodal perception. A public repository contains the CAD files to build a camera, the measured RIRs and the configurable python scripts to capture new RIRs if necessary ¹.

B. Voice activity detection

At its core, the VAD module uses a small recurrent neural network. As shown in figure 4, the network consists of two gated recurrent units (GRU) layers so that it can extract patterns over time, a linear layer to synthesize the information from the latent space and a sigmoid to scale the output between 0 and 1.

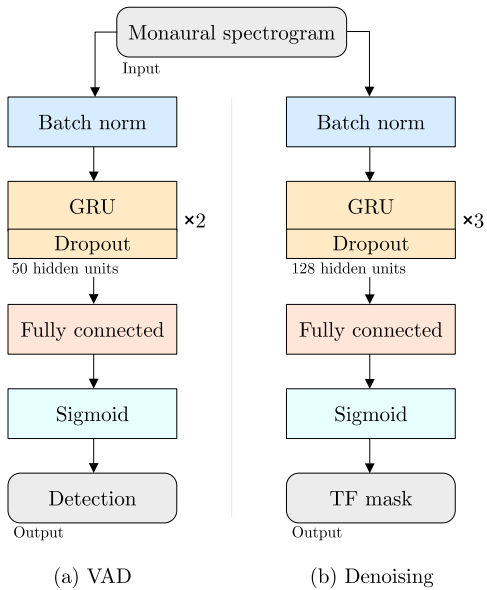


Fig. 4. Architecture of the neural networks used for the VAD module (a) and the denoising module (b). The network used for the VAD has 61 703 trainable parameters while the denoising network has 379 907 trainable parameters. Lightweight networks are desirable to achieve real-time performances.

The VAD neural network is trained on 400 hours of audio obtained through the data augmentation pipeline presented in figure 5. Most of the samples contain vocals from LibriSpeech [20], mixed with noise from FSD50K [21], classical music from MusicNet [22] or white noise artificially generated. The rest of the dataset is made of samples containing either only voice or only noise. As music tends to generate more false alarms when compared to the other noise types, samples are generated more often with music as background noise than with other noise types.

During data augmentation, each voice sample and noise sample is randomly rolled (circular time shift) to introduce diversity in time alignment. Silence is inserted in every 1 out of 2 voice samples so that the model learns that speech can be discontinuous. The samples are convolved with random measured RIRs. Finally, the SNR is chosen in the interval $[-10, +20]$ dB, and the signals are added together. The

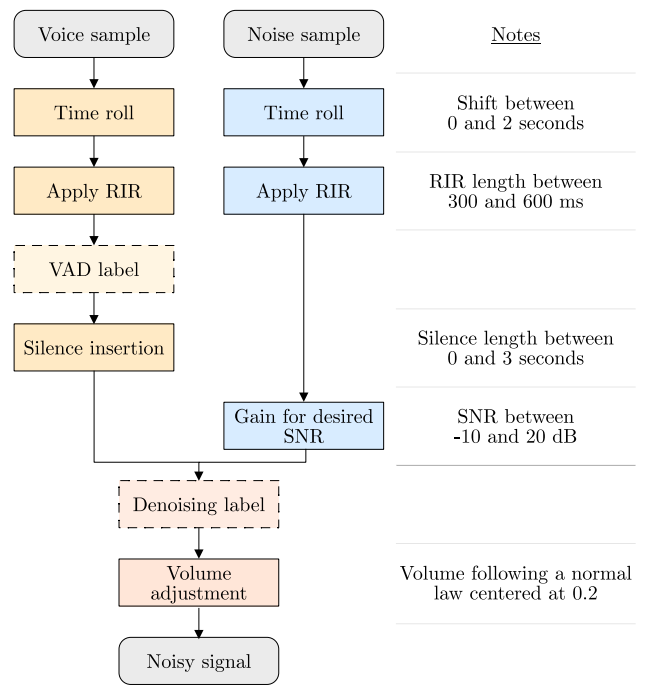


Fig. 5. Data augmentation pipeline used to generate samples to train the VAD module and the denoising module. Distribution of the samples: 10% voice only, 15% noise only, 40% voice + FSD50K noise, 30% voice + MusicNet noise and 5% voice + white noise.

volume is adjusted following a Gaussian distribution, which parameters were obtained from preliminary recordings made with the camera.

Equations 1-3 show the process to obtain the training target (VAD label) from the voice samples. The energy of each STFT time frame is first compared to the first quartile of the energy of all the time frames. If the value for a given frame is above the first quartile, it is assumed that this frame contains voice. This works because a good portion of the time frames contains voice. That is also why the target is generated before the silence insertion (the label is adjusted to match the silence afterward). A moving average over 10 time frames is then applied to the label to make it robust to short breaks. Finally, the target is binarized with a threshold set at 0.5:

$$VAD_N[t] = \begin{cases} 1, & E[t] \geq Q_1 \\ 0, & E[t] < Q_1 \end{cases}, \quad (1)$$

$$VAD_D[t] = \frac{1}{10} \sum_{j=t-9}^t VAD_N[j], \quad (2)$$

$$VAD[t] = \begin{cases} 1, & VAD_D[t] \geq 0.5 \\ 0, & VAD_D[t] < 0.5 \end{cases}, \quad (3)$$

where $E[t]$ is the energy of the time frame t , Q_1 is the first quartile of the energy of all the frames, VAD_N is the noisy label, VAD_D is the desensitized label and VAD is the training label.

¹<https://github.com/introlab/echolense>

A binary cross-entropy loss function is used and the model is trained over 100 epochs with the Adam optimizer, a batch size of 64 and a learning rate of 0.001. The final model obtained an accuracy score of 93.4% on the validation dataset. Figure 6 shows an example of VAD predicted by the model on data recorded with the acoustic camera.

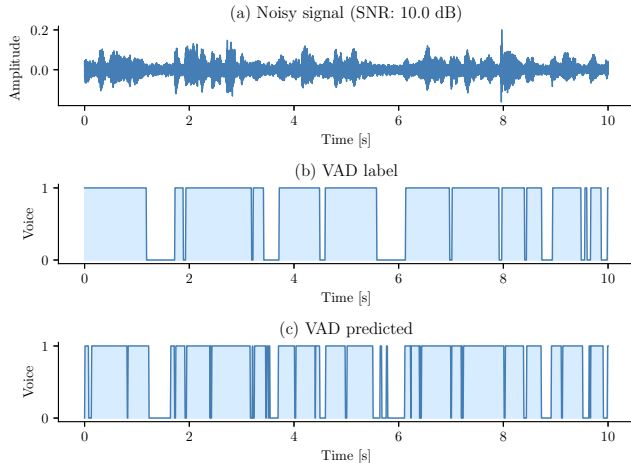


Fig. 6. Example of VAD made by the module at a SNR of 10 dB. The output of the network is binarized with a threshold set at 0.3.

C. Denoising

As shown in figure 4, the denoising module uses a neural network similar to the VAD module. The main difference is that the GRU layers contain more hidden units since the task is more complex: the model needs to generate a time-frequency (TF) mask from a given spectrogram to attenuate the noise bins and preserve the voice using (4). Here \hat{S}_s and X_s are the spectra of the denoised signal and noisy signal, respectively, and k is the frequency bin index, t is the frame index and M is the time-frequency mask:

$$\hat{S}_s[t, k] = M[t, k]X_s[t, k]. \quad (4)$$

As opposed to the speech enhancement systems, the predicted mask can introduce distortions in the reconstructed speech signal, as long as it produces accurate localization results. After experimenting with the different types of masks listed in [23], we found out that the combination of (5) and (6) provides the best localization results for this application:

$$M_{soft}[t, k] = \frac{|S_s[t, k]|^2}{|X_s[t, k]|^2} \cos(\angle S_s[t, k] - \angle X_s[t, k]), \quad (5)$$

$$M[t, k] = \begin{cases} 1, & M_{soft}[t, k] \geq 0.5 \\ 0, & M_{soft}[t, k] < 0.5 \end{cases}, \quad (6)$$

where S_s is the spectrum of the voice signal, \angle stands the phase of a complex number, M_{soft} is a phase sensitive mask and M is a binarized version of it and the training target. The choice of (5) is also confirmed in [24] for a similar task.

The model is trained with the same parameters as the VAD module. It produces an accuracy score of 85.3% on

the validation dataset. Figure 7 shows examples of masks estimated by the network.

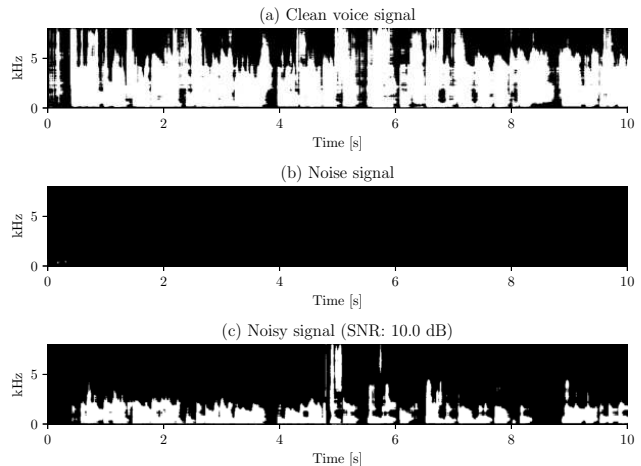


Fig. 7. Examples of masks generated by the denoising module at an SNR of 10 dB. The masks are binarized with a threshold set at 0.7. A 0 is represented by black and a 1 is represented by white.

D. Acoustic images

The acoustic image is generated using the SVD-PHAT method [25]. In this work, the resolution of the acoustic image is set to be 9×7 regions (as shown in Fig. 2). The average cross-spectrum with phase transform between each pair of microphones denoted by indexes i and j is obtained recursively using the denoising mask $M[t, k]$:

$$X_{i,j}[t, k] = (1 - \alpha)X_{i,j}[t - 1, k] + \alpha M[t, k]\hat{X}_{i,j}[t, k], \quad (7)$$

where

$$\hat{X}_{i,j}[t, k] = \frac{X_i[t, k]X_j[t, k]^*}{|X_i[t, k]||X_j[t, k]|}, \quad (8)$$

and α is the adaptive rate, and $\{ \dots \}^*$ stands for the complex conjugate operator. The SVD-PHAT method generates efficiently the acoustic image for each region using a low-rank projection matrix and a supervector that holds the cross-spectra for all pairs and frequency bins [26]. The region with the maximum acoustic energy corresponds to the sound source position.

IV. EXPERIMENTAL RESULTS

A. Evaluation dataset

We validated the proposed approach in realistic conditions using a dataset of 500 videos generated from recordings made with the acoustic camera. The recordings include 6 individuals (3 males / 3 females) reading prompts in french at different positions in front of the acoustic camera, and 3 noise sources: jiggling keys, a hairdryer blowing and classical music playing in a loudspeaker. This gives a total of 117 voice recordings and 221 noise recordings divided in 3 rooms. For every recording, the images were captured at a

rate of approximately 15 frames per second, with a resolution of 640×480 pixels.

The audio of each video in the dataset was generated by randomly selecting a voice sample and a noise sample from the same room, and by mixing them together at a desired SNR. The volume is set to 0.2. The images of the videos come from the voice recordings and contain only the face of the individuals speaking.

B. Modules validation

To evaluate the VAD, we used equations 1-3 on the dataset to determine the targets and compare them to the output of the module. At a time-frame level, the dataset is unbalanced as more frames contain voice. Therefore, to get a representative overview of the model, we use the accuracy, the sensitivity and the specificity as metrics. We also measure the specificity on the noise recordings to determine if the model had more difficulties with certain types of noise. Table I shows the results.

TABLE I
PERFORMANCE OF THE VAD MODULE AT A DECISION THRESHOLD OF 0.3 IN VARIOUS CONDITIONS

Types of samples	Accuracy	Sensitivity	Specificity
Mix @ SNR 20 dB	0.8493	0.8708	0.7641
Mix @ SNR 10 dB	0.8385	0.8651	0.7333
Mix @ SNR 0 dB	0.7858	0.8184	0.6567
Jiggling keys only	-	-	0.9425
Hairdryer only	-	-	0.6948
Music only	-	-	0.5018

According to these results, the VAD module seems biased toward detecting voices and generating false positives. This behavior is more desirable than the opposite (generating false negatives) as it forces the system to generate ROIs in case of doubt. This explains why the threshold is set to a low value (0.3 in this case). This bias could also be due to the training dataset being imbalanced at a time-frame level, but further investigations are needed to confirm this with certainty.

The performance of the denoising module for localization purpose is evaluated by measuring the average distance (in pixels) between the estimated direction of arrival (DoA) of the clean voice and the estimated DoAs of the noisy and denoised signals for each video frame. A paired t-test is also performed to ensure the validity of the observed difference. Table II shows the results. Results confirm that the denoising module is able to reduce the distance by a significant amount even in low SNR.

C. System evaluation

YuNet [27] performs face detection here. In the baseline configuration, the face detection module processes each frame completely. For the other configurations, the module scans the ROIs only. The ROIs has a size of 250×250 pixels. To test for the worst case scenarios, all frames are processed regardless of the VAD output.

TABLE II
PERFORMANCE OF THE DENOISING MODULE AT A DECISION THRESHOLD OF 0.7 IN VARIOUS CONDITIONS

SNR	Distance from clean signal DoA		t-test	$p < 0.05$
	Noisy signal	Denoised signal		
20 dB	75.10 px	38.94 px	11.44	Yes
15 dB	122.79 px	57.73 px	15.88	Yes
10 dB	165.66 px	84.50 px	18.05	Yes
5 dB	201.08 px	117.14 px	18.76	Yes
0 dB	231.42 px	152.87 px	16.12	Yes

To determine how the system compared in terms of computational load, we measure the average runtime and the average number of floating-point operations (FLOPs) to process each video frame in the dataset. The runtime is measured with `perf_counter()` from the Python time module while the FLOPs are measured by summing the results of the `PAPI_SP_OPS` and `PAPI_DP_OPS` events of PAPI². The estimations by PAPI can vary for the same amount of input data, and the results shown correspond to an average made over numerous runs. Table III shows the different configurations studied and their score. The full pipeline was able to reduce the runtime by 52% which is considerable.

TABLE III
AVERAGE RUNTIME AND NUMBER OF FLOPs OF THE SYSTEM TO PROCESS A SINGLE VIDEO FRAME

Configuration	Runtime		MFLOPs		
	ms	Gain	YuNet	Pipeline	Total
F (baseline)	17.60	1.00	70.71	-	70.71
F + L	5.81	3.03	24.70	0.57	25.27
F + L + D	8.52	2.06	21.40	2.94	24.34
F + L + D + V	9.18	1.92	20.03	3.63	23.66

F = Face detection; L = Localization; D = Denoising; V = VAD

The results for the number of FLOPs show that the pipeline can reduce the number of operations by a factor of approximately 2.80 which is considerable. It is also worth noticing that the region proposals mechanism involves a small number of computations compared to YuNet. These results confirm that processing audio in order to make ROIs has potential in order to improve processing speed.

To determine how relevant the ROIs are, we count the total number of faces that YuNet could detect on full video frames and compare this number to the total count of faces detected on the ROIs. The results are compiled in table IV.

In high SNR, the pipeline was able to capture more than 80% of the faces initially detected. In lower SNR, the denoising module becomes mandatory as it increases the relevancy of the ROIs significantly.

²<https://icl.utk.edu/papi/>

TABLE IV

TOTAL NUMBER OF FACES DETECTED AND PERCENTAGE RELATIVE TO BASELINE

SNR	Baseline	No denoising		Denoising	
35 dB	72 632	64 475	88.77%	61 446	84.60%
30 dB	72 632	63 419	87.32%	60 824	83.74%
25 dB	72 632	60 772	83.67%	59 156	81.45%
20 dB	72 632	54 158	74.56%	56 914	78.36%
15 dB	72 632	44 478	61.24%	53 070	73.07%
10 dB	72 632	35 071	48.29%	46 217	63.63%
5 dB	72 632	28 156	38.77%	39 270	54.07%
0 dB	72 632	22 683	31.23%	33 890	46.66%

V. CONCLUSION

In this paper, we proposed a unique pipeline to make region proposals for image face detection based on audio and showed that it reduces significantly the amount of computations. As future work, it would be relevant to 1) train the models on more dynamic noise sources; 2) replace the VAD module by a SNR estimator to create strategies on when to engage the denoising module; 3) explore with bigger ROIs or develop strategies to search for a face from the initial region proposals; and 4) explore low-dimensional audio input features to reduce the number of parameters in the neural networks.

REFERENCES

- [1] Y. Le Cun, B. Boser, J. S. Denker, R. E. Howard, W. Hubbard, L. D. Jackel, and D. Henderson, "Handwritten digit recognition with a back-propagation network," in *Advances in neural information processing systems 2*. Morgan Kaufmann Publishers Inc., 1990, pp. 396–404.
- [2] J. Canny, "A computational approach to edge detection," *IEEE Transactions on Pattern Analysis and Machine Intelligence*, vol. 8, no. 6, pp. 679–698, 1986.
- [3] P. Viola and M. Jones, "Rapid object detection using a boosted cascade of simple features," in *Proceedings of the IEEE Computer Society Conference on Computer Vision and Pattern Recognition*, vol. 1, 2001, pp. 511–518.
- [4] M. Aqqa, P. Mantini, and S. Shah, "Understanding how video quality affects object detection algorithms," in *Proceedings of the International Joint Conference on Computer Vision, Imaging and Computer Graphics Theory and Applications*, 2019, pp. 96–104.
- [5] J. R. R. Uijlings, K. E. A. van de Sande, T. Gevers, and A. W. M. Smeulders, "Selective search for object recognition," *International Journal of Computer Vision*, vol. 104, no. 2, pp. 154–171, 2013.
- [6] S. Ren, K. He, R. Girshick, and J. Sun, "Faster R-CNN: Towards real-time object detection with region proposal networks," in *Advances in Neural Information Processing Systems*, vol. 28, 2015.
- [7] T. Kong, A. Yao, Y. Chen, and F. Sun, "HyperNet: Towards accurate region proposal generation and joint object detection," in *Proceedings of the IEEE Conference on Computer Vision and Pattern Recognition*, 2016, pp. 845–853.
- [8] J. Hosang, R. Benenson, and B. Schiele, "How good are detection proposals, really?" *arXiv preprint arXiv:1406.6962*, 2014.
- [9] C. L. Zitnick and P. Dollár, "Edge boxes: Locating object proposals from edges," in *Proceedings of the European Conference on Computer Vision*, 2014, pp. 391–405.
- [10] C. Zhang, P. Yin, Y. Rui, R. Cutler, P. Viola, X. Sun, N. Pinto, and Z. Zhang, "Boosting-based multimodal speaker detection for distributed meeting videos," *IEEE Transactions on Multimedia*, vol. 10, no. 8, pp. 1541–1552, 2008.
- [11] L. Lacheze, Y. Guo, R. Benosman, B. Gas, and C. Couverture, "Audio/video fusion for objects recognition," in *Proceedings of the IEEE/RSJ International Conference on Intelligent Robots and Systems*, 2009, pp. 652–657.
- [12] T. Giannakopoulos, A. Makris, D. Kosmopoulos, S. Perantonis, and S. Theodoridis, "Audio-visual fusion for detecting violent scenes in videos," in *Proceedings of the Hellenic Conference on Artificial Intelligence: Theories, Models and Applications*, 2010, pp. 91–100.
- [13] B. Kapralos, M. R. Jenkin, and E. Milios, "Audiovisual localization of multiple speakers in a video teleconferencing setting," *International Journal of Imaging Systems and Technology*, vol. 13, no. 1, pp. 95–105, 2003.
- [14] B. H. Yoshimi and G. S. Pingali, "A multimodal speaker detection and tracking system for teleconferencing," in *Proceedings of the ACM International Conference on Multimedia*, 2002, pp. 427–428.
- [15] M. Barnard, W. Wang, J. Kittler, S. M. Naqvi, and J. Chambers, "Audio-visual face detection for tracking in a meeting room environment," in *Proceedings of the International Conference on Information Fusion*, 2013, pp. 1222–1227.
- [16] C. Knapp and G. Carter, "The generalized correlation method for estimation of time delay," *IEEE Transactions on Acoustics, Speech, and Signal Processing*, vol. 24, no. 4, pp. 320–327, 1976.
- [17] R. Schmidt, "Multiple emitter location and signal parameter estimation," *IEEE Transactions on Antennas and Propagation*, vol. 34, no. 3, pp. 276–280, 1986.
- [18] J. H. DiBiase, *A high-accuracy, low-latency technique for talker localization in reverberant environments using microphone arrays*. Brown University, 2000.
- [19] A. Farina, "Simultaneous measurement of impulse response and distortion with a swept-sine technique," in *Proceedings of the Audio Engineering Society Convention*, 2000.
- [20] V. Panayotov, G. Chen, D. Povey, and S. Khudanpur, "Librispeech: An ASR corpus based on public domain audio books," in *Proceedings of the IEEE International Conference on Acoustics, Speech and Signal Processing*, 2015, pp. 5206–5210.
- [21] E. Fonseca, X. Favory, J. Pons, F. Font, and X. Serra, "FSD50K: An open dataset of human-labeled sound events," *IEEE/ACM Transactions on Audio, Speech, and Language Processing*, vol. 30, pp. 829–852, 2022.
- [22] J. Thickstun, Z. Harchaoui, and S. M. Kakade, "MusicNet," 2016. [Online]. Available: <https://zenodo.org/record/5120004>
- [23] H. Erdogan, J. R. Hershey, S. Watanabe, and J. Le Roux, "Phase-sensitive and recognition-boosted speech separation using deep recurrent neural networks," in *Proceedings of the IEEE International Conference on Acoustics, Speech and Signal Processing*, 2015, pp. 708–712.
- [24] Z.-Q. Wang, X. Zhang, and D. Wang, "Robust speaker localization guided by deep learning-based time-frequency masking," *IEEE/ACM Transactions on Audio, Speech, and Language Processing*, vol. 27, no. 1, pp. 178–188, 2019.
- [25] F. Grondin, H. Tang, and J. Glass, "Audio-visual calibration with polynomial regression for 2-D projection using SVD-PHAT," in *Proceedings of the IEEE International Conference on Acoustics, Speech and Signal Processing*, 2020, pp. 4856–4860.
- [26] F. Grondin and J. Glass, "SVD-PHAT: A fast sound source localization method," in *Proceedings of the IEEE International Conference on Acoustics, Speech and Signal Processing*, 2019, pp. 4140–4144.
- [27] W. Wu, H. Peng, and S. Yu, "YuNet: A tiny millisecond-level face detector," *Machine Intelligence Research*, pp. 1–10, 2023.